Mantle Petrology: Field Observations and High Pressure Experimentation: A Tribute to Francis R. (Joe) Boyd
© The Geochemical Society, Special Publication No. 6, 1999
Editors: Yingwei Fei, Constance M. Bertka, and Bjorn O. Mysen

Effect of pressure on the fractional crystallization of basaltic magma

DEAN C. PRESNALL
Magmalogy Laboratory, Department of Geosciences, University of Texas at Dallas, P.O. Box 830688, Richardson, TX 75083, U.S.A.

Abstract—In the CaO-MgO-Al_2O_3-SiO_2 system, algebraic calculations based on liquidus phase relations in the tetrahedron forsterite-diopside-anorthite-silica at 1 atm, 2 GPa, and 3 GPa are used to develop simplified quantitative models for fractional crystallization of basaltic magma as a function of pressure. At 1 atm, an initial olivine-controlled trend is followed successively by crystallization of forsterite + anorthite, forsterite + anorthite + diopside, enstatite + diopside + anorthite, and enstatite + diopside + anorthite + quartz. At 2 GPa, the initial olivine-controlled trend is abbreviated, and spinel, sapphirine, and garnet appear in the middle stages of fractionation. At 3 GPa, diopside and garnet are the main crystallizing minerals along with minor spinel, sapphirine, corundum and kyanite. At all pressures, residual liquids are strongly enriched in SiO_2 and the maximum SiO_2 enrichment decreases with pressure. Also, MgO is strongly depleted at all pressures and the amount of depletion increases with pressure. At 1 atm, CaO initially increases but then decreases when diopside begins to crystallize. At higher pressures, diopside appears early, which suppresses early CaO enrichment. Early anorthite crystallization at 1 atm causes Al_2O_3 to decrease, but at 2 GPa, the late appearance of anorthite slightly suppresses Al_2O_3 only after strong early enrichment. At 3 GPa, Al_2O_3 enrichment is even stronger. At least for the middle and late portions of the fractionation trends at spreading ridges and at Hawaii, the data strongly support conventional models involving extensive fractional crystallization at very low pressures. The early olivine-controlled portion of the Hawaii trend could be produced either by low pressure crystallization or polybaric crystallization from picritic parental magmas. Also, the early part of the trend at spreading ridges appears to be affected by fractional crystallization at elevated pressures. Although water is abundant and amphibole is widespread as a crystallization product from arc magmas, the high Al_2O_3 and low MgO signatures of these magmas appear to be most strongly controlled by the existence of high pressures during fractional crystallization.

INTRODUCTION

THE BASALT tetrahedron, olivine-clinopyroxene-nepheline-quartz, of YODER and TILLEY (1962) has been used extensively for representation of basalt compositions and discussions of the chemical evolution of basalts. The tetrahedron, forsterite (Mg_2SiO_4) - anorthite ($CaAl_2Si_2O_8$) - diopside ($CaMgSi_2O_6$) - silica (SiO_2) (FADS) in the four-component system CaO-MgO-Al_2O_3-SiO_2 (CMAS) (Fig. 1), has been used as a simplified version of the tholeiitic portion of the basalt tetrahedron. It is particularly attractive for modeling the generation of basalts from a lherzolitic mantle because it shows primary phase volumes representative of all the major lherzolite minerals (forsterite, enstatite, diopside, anorthite, spinel, garnet), as well as the progressive change in mineralogy of the mantle from plagioclase lherzolite through spinel lherzolite to garnet lherzolite as pressure increases (Fig. 2). Additionally, about 85% of the composition of basalts and about 90% of the composition of the mantle source can be represented. The tetrahedron has been used extensively to model the generation of basaltic liquids (O'HARA, 1965, 1968; O'HARA and YODER, 1967; KUSHIRO, 1968, 1969, 1975; YODER, 1976; PRESNALL *et al.*, 1978; 1979; HERZBERG, 1992; WALTER and PRESNALL, 1994; GUDFINNSSON and PRESNALL, 1996; HERZBERG and ZHANG, 1997; HERZBERG and O'HARA, 1998); and the close correspondence of lherzolite melting reactions in the CMAS system to those for more complex model systems and for natural compositions (MILHOLLAND and PRESNALL, 1998) emphasizes the usefulness of this simple system as a model for understanding and predicting the melting behavior of natural lherzolite at various pressures.

The FADS tetrahedron has also been used for modeling trends of fractional crystallization of tholeiitic basalts (*e.g.*, O'HARA, 1965, 1968; O'HARA and YODER, 1967; O'DONNELL and PRESNALL, 1980; PRESNALL and HOOVER, 1987), including picrites and komatiites (MILHOLLAND and PRESNALL, 1998); but due to the absence of several components such as iron oxides and alkalies, some aspects of the fractionation of natural basaltic magmas cannot be addressed. Nevertheless, the phase relations provide an important guide to the effect of pressure on the trends for CaO, MgO, Al_2O_3, and SiO_2. The purpose of this paper is to show the effect of pressure on fractional crystallization paths of model basaltic liquids in this system and to briefly examine the implications of these paths for fractional crystallization processes at oceanic spreading centers, at Hawaii, and at subduction zones. The discussion will consider fractional crystallization at pressures only up to 3 GPa. At

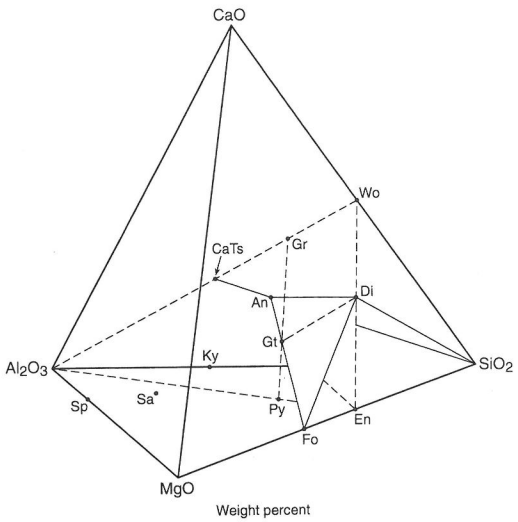

FIG. 1. The tetrahedron CaO-MgO-Al_2O_3-SiO_2 showing the model tholeiitic basalt tetrahedron Fo-Di-An-SiO_2. Dashed lines lie in the aluminous pyroxene thermal divide, Wo-En-Al_2O_3. Abbreviations are as follows: Sp, spinel ($MgAl_2O_4$); Sa, sapphirine ($Mg_2Al_4SiO_{10}$); Ky, kyanite (Al_2SiO_5); CaTs, Ca Tschermak's molecule ($CaAl_2SiO_6$); An, anorthite ($CaAl_2Si_2O_8$); Gt, garnet ($CaMg_2Al_2Si_3O_{12}$); Gr, grossular ($Ca_3Al_2Si_3O_{12}$); Py, pyrope ($Mg_3Al_2Si_3O_{12}$); Wo, wollastonite ($CaSiO_3$); Di, diopside ($CaMgSi_2O_6$); En, enstatite ($MgSiO_3$); Fo, forsterite (Mg_2SiO_4).

greater pressures, the aluminous pyroxene thermal divide, first proposed by YODER and TILLEY (1962) and O'HARA and YODER (1963), causes the production of silica undersaturated residual liquids distinct from those produced at pressures less than 3 GPa and discussed here. Fractional crystallization at pressures greater than this thermal divide was discussed extensively by O'HARA and YODER (1967), and new data clarifying some of the relevant phase relations have recently been presented by MILHOLLAND and PRESNALL (1998).

The most serious problem in the application of phase relations in the FADS tetrahedron to the fractional crystallization of basaltic magmas at various pressures is the absence of iron oxides and the alkalies, especially Na_2O. The effects of iron oxides at 1 atm have been extensively studied in the systems MgO-FeO-Fe_2O_3-SiO_2 (MUAN and OSBORN, 1956; OSBORN, 1959), MgO-FeO-Fe_2O_3-SiO_2-CaO (PRESNALL, 1966), and MgO-FeO-Fe_2O_3-SiO_2-CaO-Al_2O_3 (ROEDER and OSBORN, 1966; SHI and LIBOUREL, 1991), but none of these systems have been studied at high pressures. The discussion presented here, although limited to four components, provides a start toward a more quantitative understanding of the effects of pressure on fractional crystallization. KUSHIRO (1976) has given an excellent review of the older literature, which will not be repeated here.

PHASE RELATIONS

Figures 3, 4, 5, 6, and 7 show primary phase volumes in the FADS tetrahedron at 1 atm, 2 GPa, and 3 GPa. One of the most important changes is the decreasing size of the forsterite primary phase volume as pressure increases. Except for the anorthite volume, this decrease occurs relative to all the primary phase volumes, enstatite, diopside, and spinel, that come in contact with the forsterite volume at pressures less than 3 GPa. At pressures above 3 GPa, the garnet volume also expands with pressure at the expense of the forsterite volume. Therefore, primary magmas, which are always generated in equilibrium with olivine in the upper mantle, become increasingly enriched in MgO as the pressure of generation increases. Other changes in liquidus primary phase volumes with increasing pressure include shrinkage of the anorthite volume, appearance and then shrinkage at higher pressures of the sapphirine volume, and appearance and continued expansion of the corundum and kyanite volumes (LIU and PRESNALL, 1990, in press; MILHOLLAND and PRESNALL, 1998).

At 2 and 3 GPa, liquidus phase relations in the FADS tetrahedron (Figs. 4 and 6) are much more complex than those at 1 atm. Because of this increased complexity, Figs. 5 and 7 are included as aids

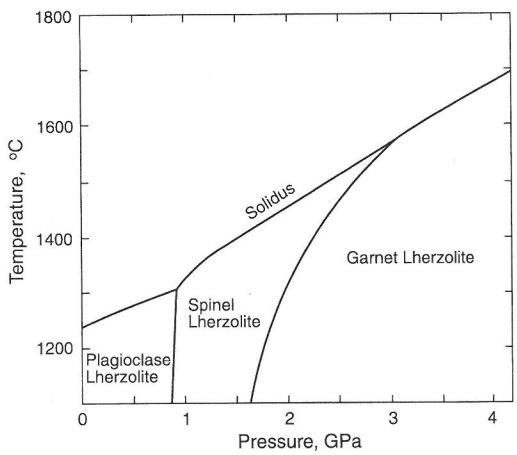

FIG. 2. Stability fields for plagioclase lherzolite (fo + en + di + an), spinel lherzolite (fo + en + di + sp), and garnet lherzolite (fo + en + di + gt) in the CaO-MgO-Al_2O_3-SiO_2 system. Compiled from DAVIS and SCHAIRER (1965), O'HARA *et al.* (1971), KUSHIRO (1972), HERZBERG (1972), PRESNALL (1976), PRESNALL *et al.* (1979), GASPARIK (1984), GUDFINNSSON and PRESNALL (1996), and MILHOLLAND and PRESNALL (1998).

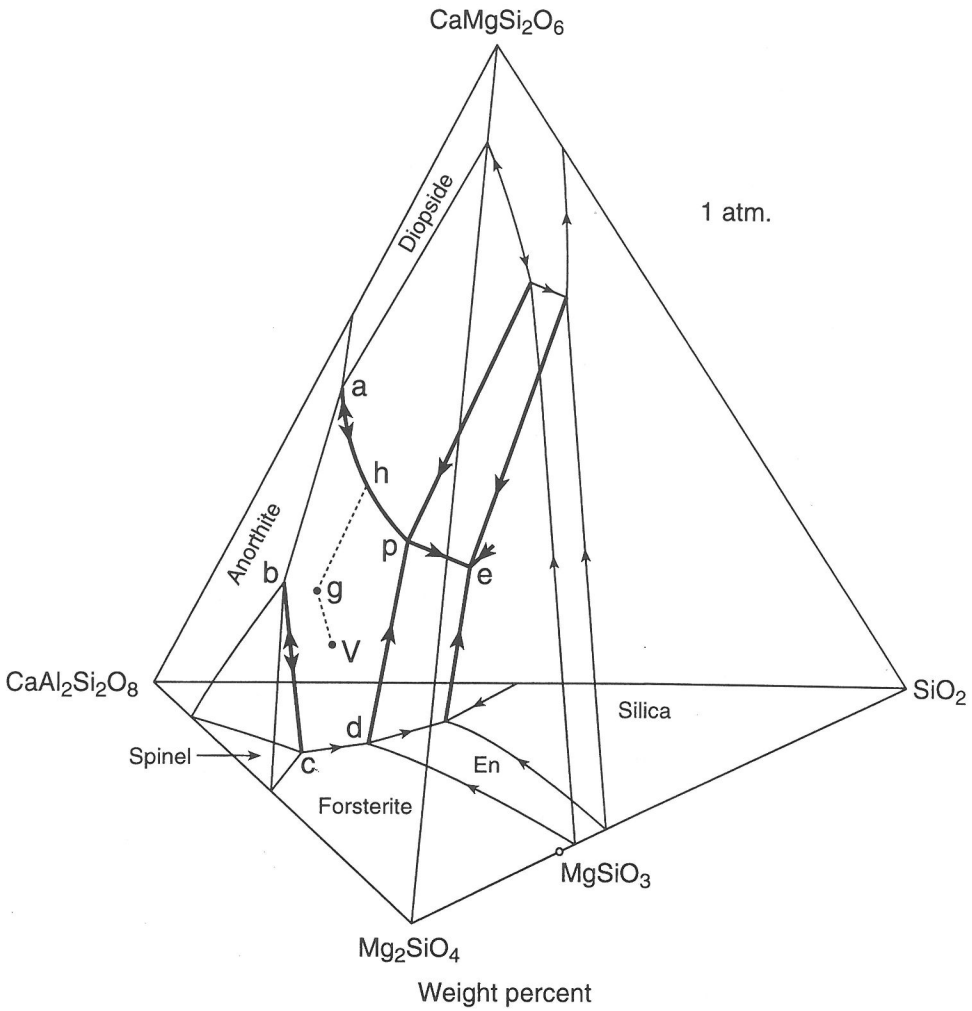

FIG. 3. Liquidus phase relations in the system forsterite-anorthite-diopside-silica at 1 atm. Compiled from BOWEN (1914), ANDERSEN (1915), OSBORN and TAIT (1952), HYTÖNEN and SCHAIRER (1961), KUSHIRO and SCHAIRER (1963), SCHAIRER and KUSHIRO (1964), KUSHIRO (1969), PRESNALL *et al.* (1979), LONGHI and HAYS (1979), LONGHI (1987), LIBOUREL *et al.* (1989), LIU and PRESNALL (1989) and WALTER and PRESNALL (1994). Light boundary lines are on the faces of the tetrahedron; heavy boundary lines are in the interior. Arrows indicate directions of decreasing temperature. The dashed line, V–g–h, is part of a liquid crystallization path (see text). Primary phase volumes for pigeonite, orthoenstatite, orthopyroxene (not the same phase as orthoenstatite), and protoenstatite do not affect the discussion of fractional crystallization and are omitted for clarity. The temperature maximum on line a–p is displaced slightly toward p from its true position due to space needed to show the arrows. The position of the temperature maximum on line b–c is based on a determinant solution involving the compositions an, fo, di, b, and c.

in visualizing the phase relations. These diagrams show the diopside-saturated liquidus surface as it would appear to a viewer looking down from the $CaMgSi_2O_6$ apex in Figs. 4 and 6.

In Fig. 4, new primary phase volumes not present at 1 atm are sapphirine, corundum, and garnet. Also, the size of the anorthite volume is significantly reduced. The very small size of the garnet volume and its greatly enlarged size at 3 GPa (Fig. 6) indicates that it first appears at a pressure only slightly below 2 GPa. At 3 GPa (Figs. 6 and 7), the sapphirine volume is smaller than at 2 GPa (Figs. 4 and 5). This suggests the existence of an upper pressure stability limit greater than 3 GPa for sapphirine at the liquidus. Existing data provide only a very crude lower pressure liquidus stability limit between 1 and 2 GPa (LIU and PRESNALL, in press).

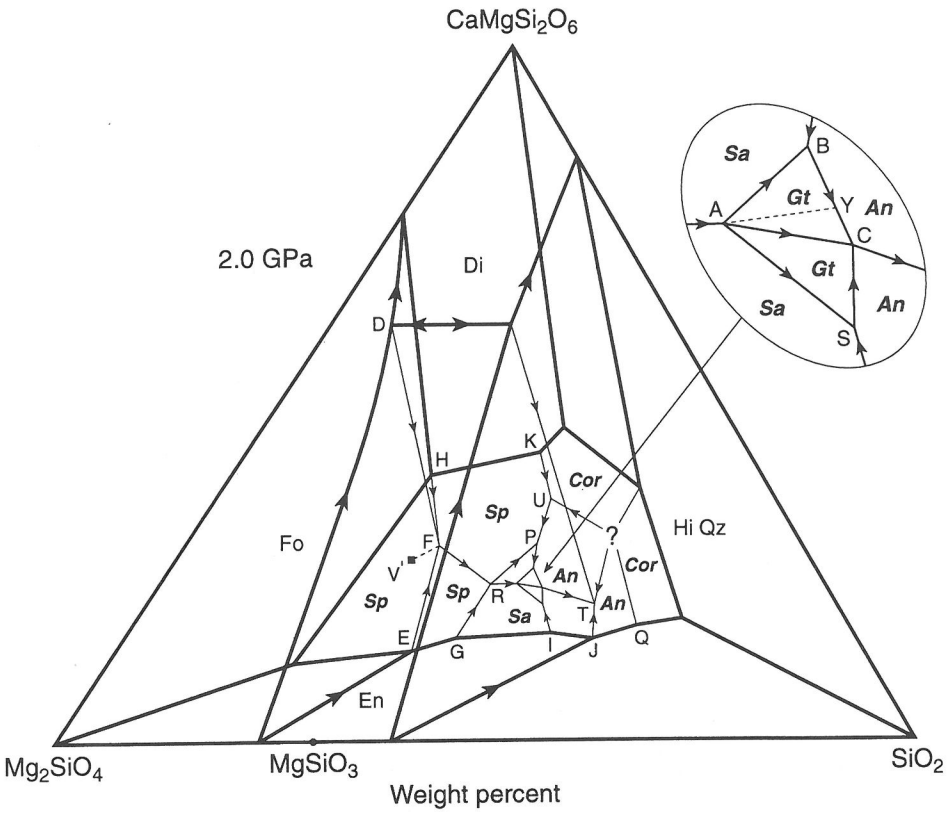

FIG. 4. Liquidus phase relations in the system forsterite-anorthite-diopside-silica at 2.0 GPa (CLARK *et al.*, 1962; KUSHIRO, 1969; PRESNALL *et al.*, 1978, 1979; LIU and PRESNALL, 1990, in press; WALTER and PRESNALL, 1994). The anorthite apex is hidden in the rear behind the faceted opaque boundary surface defined by the corundum, anorthite, garnet, sapphirine, and spinel primary phase volumes. Phase boundaries occur behind the opaque surface that are not visible in this representation. Boundary surfaces between the pyroxene and forsterite primary phase volumes and between the pyroxene and high quartz volumes are transparent in order to reveal phase relations in the rear of the tetrahedron. Heavy boundary lines are in the faces of the tetrahedron; light boundary lines are in the interior. Arrows indicate directions of decreasing temperature. Bold italic labels indicate the primary phase volume behind the surface containing the label. Ordinary labels are within primary phase volumes toward the front of the tetrahedron. Line A–Y in the inset is part of a crystallization path (see text). Cor, corundum; Hi Qz, high quartz. Other abbreviations as in Fig. 1.

At pressures above 3 GPa, the aluminous pyroxene thermal divide (Al_2O_3-$CaSiO_3$-$MgSiO_3$, Fig. 1) causes crystallization paths profoundly different from those followed at pressures below 3 GPa. Below this pressure, the thermal divide has no effect. As pressure increases from 3 GPa, the thermal divide becomes increasingly effective, as discussed by MILHOLLAND and PRESNALL (1998).

FRACTIONAL CRYSTALLIZATION PATHS

For binary and ternary systems, classical geometrical procedures are well suited for rapid and quantitative determination of crystallization paths. In a four-component system, such procedures can still be used, but they are typically cumbersome because a three-dimensional model is frequently needed. Although a perspective view of quaternary phase relations (Figs. 3, 4, 6) is visually very useful, many quantitative details of critical importance cannot be recovered. However, when a perspective view is combined with algebraic calculations, the result can be both visually and quantitatively satisfying. Of course, when systems of more than four components are considered, a generalized phase diagram can no longer be used; algebraic calculations are the only recourse.

In principle, a fractional crystallization path in a multicomponent system can be calculated in as much

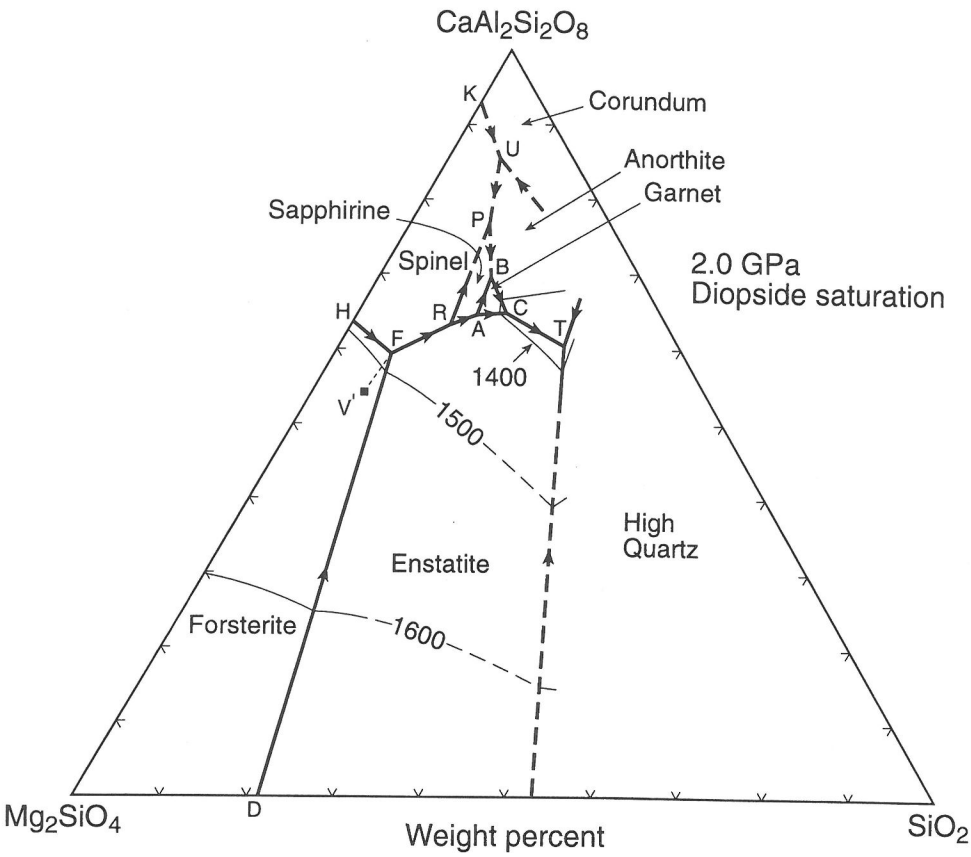

FIG. 5. Diopside saturation surface of the system forsterite-anorthite-diopside-silica at 2.0 GPa, as viewed from the $CaMgSi_2O_6$ apex of Fig. 4 (LIU and PRESNALL, in press). All liquidus phase fields have diopside in addition to the phase indicated. Arrows indicate directions of decreasing temperature. Temperatures are in °C.

detail as desired by solving a series of balanced chemical equations, each of which describes a very small segment of the path (PRESNALL, 1986, 1991). Although high accuracy in these calculations requires dense data coverage and parameterization of all phase compositions that vary, a good understanding of the general features of fractional crystallization can frequently be obtained by using a simplified version of this procedure that involves solution of only a few determinants for the entire crystallization path. The simplified procedure is adopted here.

In order to illustrate the effects of pressure on fractional crystallization paths in the FADS tetrahedron, point V (Figs. 3, 6) is chosen as the starting composition because it is the initial liquid generated from a model garnet/spinel lherzolite at 3 GPa (MILHOLLAND and PRESNALL, 1998). At the high pressure extreme, the discussion will model the situation in which a melt is generated at 3 GPa and then fractionally crystallizes in place without rising to the earth's surface. At the other extreme, the melt is generated at 3 GPa, rises to a location very near the earth's surface, and then fractionally crystallizes at approximately 1 atm. A third case will also be discussed in which ascent of the melt generated at 3 GPa is arrested at an intermediate depth and fractional crystallization occurs at 2 GPa.

At 1 atm and 2 GPa, the phase relations are sufficiently simple that the general features of fractional crystallization paths can be quantified fairly accurately by using large algebraic steps along the paths. Representative errors associated with the use of large steps are evaluated in the discussion at 2 GPa, and it is shown that the results are relatively insensitive to this approximation. At 3 GPa, complications in the phase relations overwhelm even the large amount of data available at this pressure (MILHOLLAND and PRESNALL, 1998), such that a number of details of the crystallization path cannot be unambiguously determined. Therefore, algebraic calculations are not done

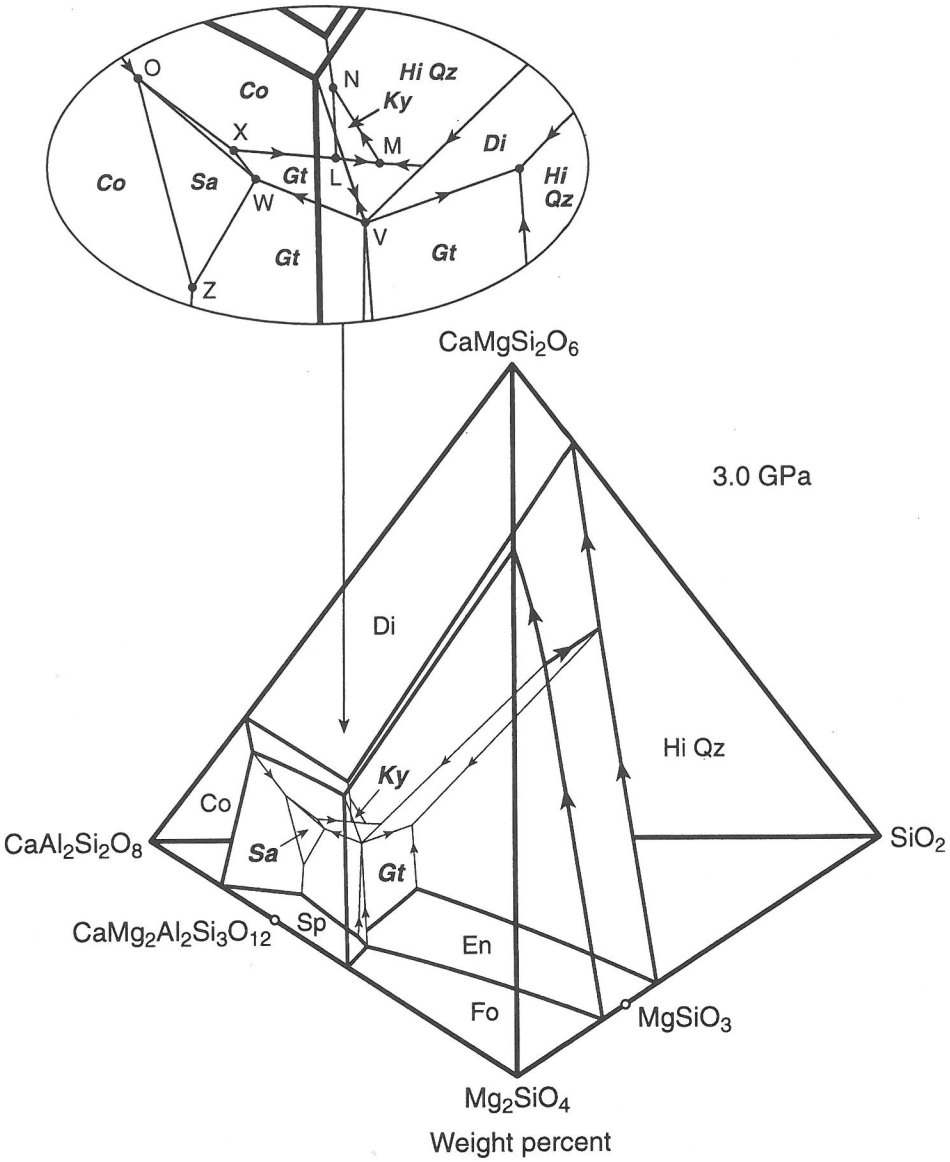

FIG. 6. Liquidus phase relations in the system forsterite-anorthite-diopside-silica at 3.0 GPa (MILHOLLAND and PRESNALL, 1998). Heavy boundary lines are on the faces of the tetrahedron; light lines are in the interior. Arrows indicate directions of decreasing temperature. Abbreviations are as in Fig. 1. Bold italic and ordinary labels have the same meaning as in Fig. 4.

at 3 GPa. Only general features of the 3 GPa crystallization path will be presented.

Fractional Crystallization at 1 Atm

Geometrical relationships involving fractional crystallization of liquid V at 1 atm are shown in Fig. 3 and the results of the calculations are shown in Fig. 8. Although liquid V is in equilibrium with forsterite, diopside, enstatite, garnet, and spinel at 3 GPa (Figs. 6, 7), rapid ascent of this model primary magma to the earth's surface would place it deep inside the expanded forsterite primary phase volume at 1 atm (Fig. 3). Thus, fractional crystallization at 1 atm begins with the precipitation of forsterite.

It is desired to determine the composition, g, where

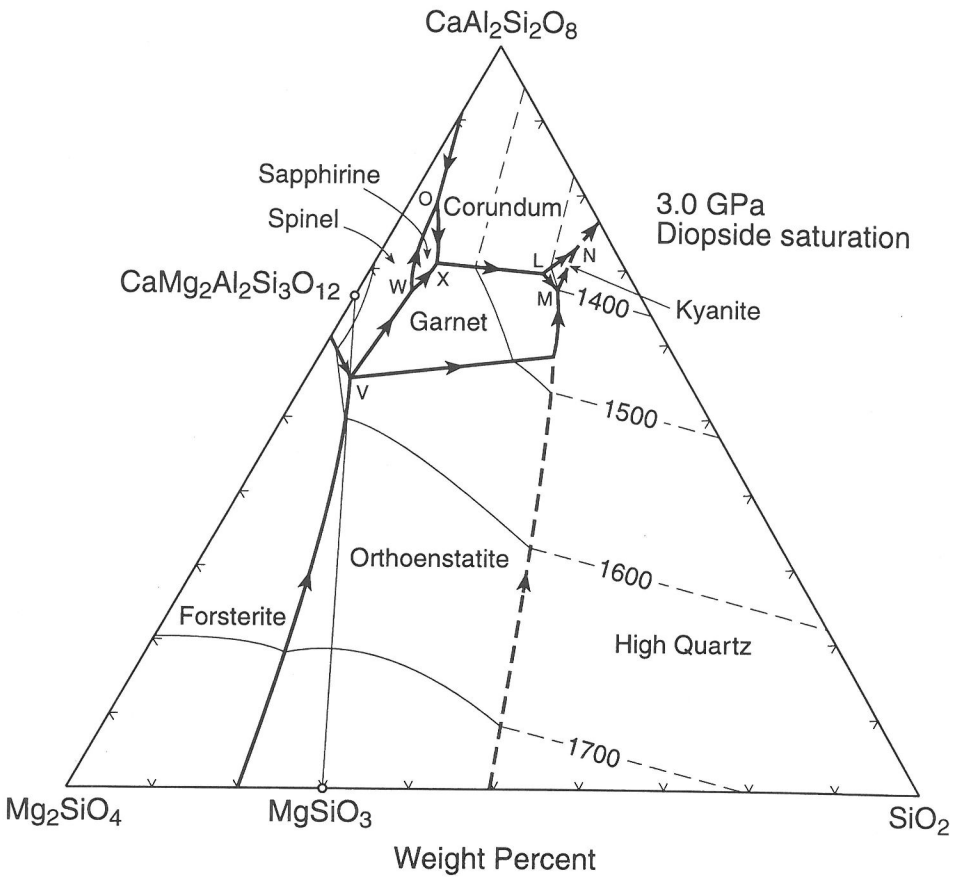

FIG. 7. Diopside saturation surface of the system forsterite-anorthite-diopside-silica at 3.0 GPa, as viewed from the $CaMgSi_2O_6$ apex of Fig. 6 (MILHOLLAND and PRESNALL, 1998). Lines and symbols as in Fig. 6.

the liquid path intersects the anorthite-forsterite surface, a–b–c–d–p (Fig. 3). This can be determined algebraically by trial and error balancing of equations using the method of KORZHINSKII (1959, p. 103–107) as applied by Presnall (1986, 1991). For a four-component system, five compositions are needed. A determinant is set up involving forsterite, liquid V, and three points on the anorthite-forsterite surface, a–b–c–d–p. Points b, c, and p on this surface are chosen as a trial, and it is assumed that the surface in the vicinity of its intersection with the liquid path can be approximated by a plane passing through these three points. For this choice, a solution is obtained in which V is alone on one side of the equation and b, c, p, and forsterite are on the other (all coefficients positive). Therefore, point g lies within the b–c–p triangle on the anorthite-forsterite surface, composition g is given by the relative proportions of b, c, and p, as defined by their coefficients, and the proportion of forsterite crystallized is given by the forsterite coefficient. However, if a poor guess had been made about the general location of g on the a–b–c–d–p surface, point V would not be alone on one side of the equation and a different set of three points on the surface would need to be tried.

The geometry of Fig. 3 indicates that liquid g moves along the a–b–c–d–p surface toward a–p as anorthite and forsterite crystallize. To quantify this, an equation is solved involving anorthite, forsterite, g, p, and a point on the a–p line. Because line a–p is slightly curved (LIBOUREL, *et al.*, 1989), an intermediate point, a′ (not shown), taken from LIBOUREL *et al.* (1989) on the a–p line slightly to the left of point h is chosen. This provides a straight-line approximation of a–p that closely matches the position of the curved line near h. Coefficients in the solution of this equation yield the composition of h as a proportion of the known compositions, p and a′, the relative pro-

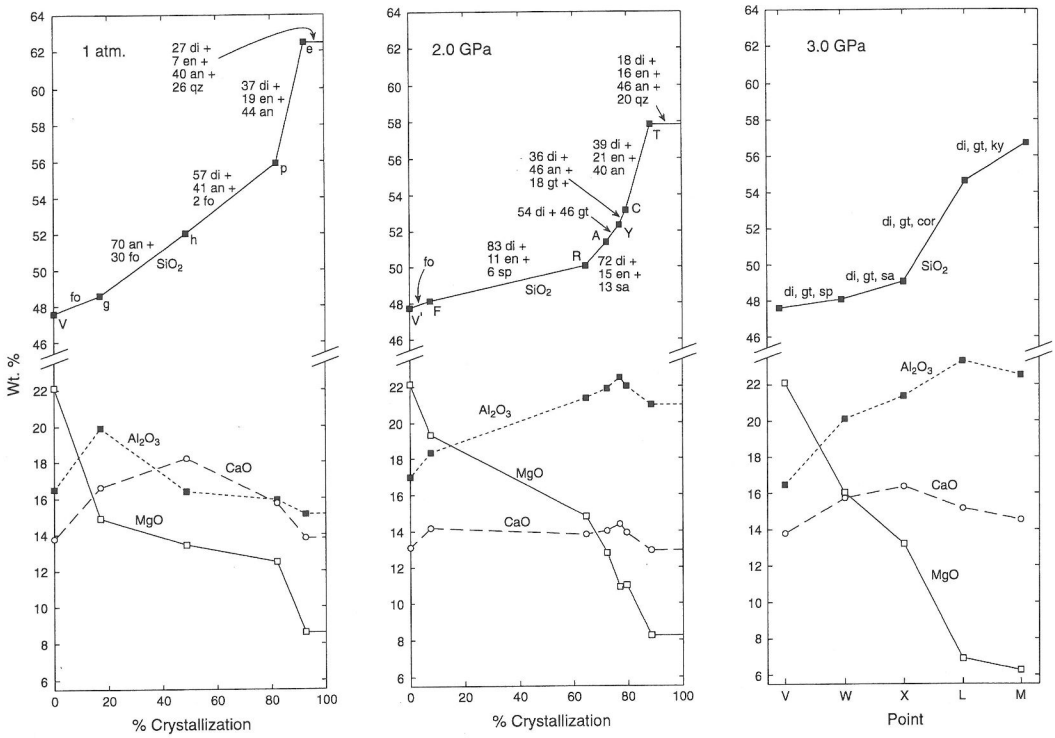

FIG. 8. Liquid compositions for fractional crystallization paths at 1 atm, 2 GPa, and 3 GPa. Labels of the points are the same as in the other figures. Crystallizing phase proportions (wt. %) are indicated for each segment of the 1 atm. and 2 GPa path.

portions of anorthite and forsterite that crystallize, and the proportion of liquid g that crystallizes just as the liquid path arrives at h (Figs. 3 and 8).

Figure 3 appears to indicate that a liquid at h moves to p by crystallization of diopside, anorthite and forsterite. However, because of solid solution in diopside, it is not evident from Fig. 7 whether forsterite crystallizes or dissolves on cooling. To determine this, the composition of diopside is taken, as an approximation, to be constant along the h–p liquid path and the same as that in equilibrium with liquid p, as determined by WALTER and PRESNALL (1994). Then, an equation is solved involving forsterite, anorthite, diopside, h, and p. The result indicates that forsterite does crystallize and makes up 2% of the crystallizing assemblage (Fig. 8). This calculation is consistent with the conclusion of LIBOUREL *et al.* (1989).

As invariant point p is a peritectic, Fig. 3 indicates that the liquid does not stop at p but moves immediately away from p, probably along p–e as enstatite, diopside, and anorthite crystallize. To test this portion of the liquid path, an equation is solved involving p (WALTER and PRESNALL, 1994), the compositions of enstatite, diopside, and liquid e determined by LONGHI (1987, Table 2), and anorthite. Solution of the equation gives the crystallizing phase proportions and amount of crystallization indicated in Fig. 8. At eutectic e, the crystallizing phase proportions of enstatite, diopside, anorthite, and quartz (Fig. 8) are determined by balancing an equation involving these five compositions and using the phase composition data given by LONGHI (1987, Table 2).

Fractional Crystallization at 2 GPa

Because of expansion of the forsterite primary phase volume as pressure decreases, liquid V lies within the forsterite volume at 2 GPa. However, this expansion is modest compared to that at 1 atm, so the amount of olivine control in the initial stage of fractional crystallization is less pronounced. Also, V is located such that crystallization of forsterite drives the residual liquid almost directly into point F (Figs. 4, 5). In order to simplify the discussion, the starting liquid V has been adjusted slightly so that crystallization of forsterite does, in fact, drive the liquid directly into F. This new starting composition is labeled V′.

Before proceeding with the algebraic discussion, it

is useful to notice that invariant point F and all other invariant points down-temperature from F are peritectics except for T, which is a eutectic. Therefore, an extensive fractional crystallization path can be anticipated, and it is expected that the final residual liquid will lie at T (Fig. 4). As simple inspection of the directions of decreasing temperature along the univariant lines suggests more than one possible route for the liquid path, and as the path may move not just along univariant lines but also across one or more divariant surfaces or even through volumes, an algebraic approach is necessary.

The initial segment of the liquid path, as explained above, involves crystallization of forsterite from V′, which drives the liquid path directly into F (Figs. 4, 8). The next segment is determined by balancing liquid F against liquid R, using the compositions of crystalline phases in equilibrium with R. As noted earlier, this yields only an approximate result because the compositions of all phases except spinel will vary slightly depending on the location of the liquid along the F–R line. In contrast to the situation at 1 atm, data are adequate at 2 GPa to examine the magnitude of the error caused by approximations of this type, as will be explained in the course of the discussion.

The initial test of F against R yields two "successful solutions" (PRESNALL, 1986), equation 1F (Table 1) and F = di + en + sa + R. Coefficients are deleted in the second equation because they are not needed in the present discussion. These two solutions are algebraic expressions of the mass-balance requirement that for any point on the liquid path followed during *equilibrium* crystallization, the bulk composition must be contained within the volume defined by the coexisting liquid and crystalline phases. Note also that the second successful solution includes sapphirine as a crystallizing phase yet this phase does not crystallize along the line F–R. This second equation indicates that the liquid path travels along line R–A as it exits point R during *equilibrium* crystallization of liquid F. However, the present discussion does not concern equilibrium crystallization, so the second successful solution will be ignored here as well as in subsequent situations of this type.

The first successful solution indicates that diopside, enstatite, and spinel crystallize in the proportions given by the coefficients and that no reaction relation occurs as the liquid path traverses the line F–R. Therefore, this initial part of the liquid path is the same for both equilibrium and fractional crystallization. If, instead of using phase compositions in equilibrium with R, phase compositions in equilibrium with F were used, the coefficients for the first successful solution would be slightly different, but the form of the equation would not change (equations 1R and 1F in Table 1). This gives a rough indication of the uncertainty produced by using large steps in the calculations. In this case, the conclusion that the liquid arrives at R after roughly 60% crystallization is not sensitive to the variations of crystalline phase

Table 1. Equations for determining fractional crystallization path at 2.0 GPa

Equation number	Path segment	Crystalline phase compositions	Equation (wt. %)
1R	F-R	At R (375-1)[1]	100F = 4sp + 7en + 51di + 38R
1F	F-R	At F[2]	100F = 5sp + 2en + 47di + 46R
2A	R-A	At A (374-7)	100R = 16di + 3en + 3sa + 78A
2R	R-A	At R (375-1)	100R = 16di + 2en + 3sa + 79A
3A	A-Y	At A (374-7)	100A = 9di + 8gt + 31B + 52C
4Y	Y-C	Near Y (383-16)	100Y = 1gt + 5di + 5an + 89C
5C	C-T	Near C (383-17)	100C = 9en + 17di + 18an + 56T
5T	C-T	At T (379-16)	100C = 12en + 14di + 22an + 52T
6T	T	At T (379-16)	100T = 15en + 18di + 47an + 21qz[3]

[1]Run numbers refer to experiments reported in Liu and Presnall (in press).
[2]From Walter and Presnall (1994).
[3]From Liu and Presnall (in press).

compositions in equilibrium with liquids along F–R. For this first segment of the crystallization path shown in Fig. 8, equation 1R (Table 1) has been arbitrarily chosen. In a more accurate calculation, equations of this type would be solved for many small segments along F–R taking into account the gradual change in phase compositions with temperature.

To determine the next segment of the liquid path followed during fractional crystallization, the starting liquid composition used in the calculation is moved to R. The univariant lines R–N and R–A both decrease in temperature away from R, but a test of R against liquid A yields the only successful solution (equations 2A and 2R in Table 1). In this case, use of crystalline phase compositions in equilibrium with either liquid R or liquid A produces nearly identical coefficients. Therefore, the liquid path moves from R to A as diopside, enstatite, and sapphirine crystallize. In Fig. 8, equation 2A is arbitrarily chosen.

When the starting composition is moved again, this time to A, three univariant lines, A–B, A–C, and A–S, decrease in temperature away from A. Because none of these yields a successful solution, it is necessary to test divariant surfaces as possibilities. One such surface is A–B–C, along which diopside and garnet crystallize. To test this surface, it is assumed, as an approximation, to be planar. As only two crystalline phases are present, liquid A is tested against two other points, B and C, on the surface plus the compositions of garnet and diopside in equilibrium with liquid A. The solution, equation 3A (Table 1), is successful. It shows that A can be expressed by positive proportions of diopside, garnet, and a liquid, Y, on the B–C boundary that lies at 37% B, 63% C. The proportions of diopside and garnet that crystallize are given by their coefficients in the equation.

The next step is to determine if the liquid path moves from Y along B–C toward C, and for this test, compositions of phases close to C are used. The equation, 4Y (Table 1) is successful and there is no reaction relationship. For the final segment from C to T, equations 5C and 5T show that enstatite, diopside and anorthite crystallize with no reaction relationship as the liquid moves along the C–T line. Again, the two equations indicate the uncertainty in the coefficients caused by using phase compositions near C versus those at T. At the quaternary eutectic, T, crystallization occurs according to reaction 6T (Table 1).

Fractional Crystallization at 3 GPa

At 3 GPa, the diopside, garnet, and corundum volumes are larger, the forsterite and sapphirine volumes are smaller, and new phases that appear during fractional crystallization are corundum and kyanite (Figs. 6 and 7). Even though the phase relations in Fig. 6 are constrained by a large amount of data (MILHOLLAND and PRESNALL, 1998), the complexities are great enough to cause a number of uncertainties in the details of crystallization paths. Therefore, the kind of quantitative calculations done above at 1 atm. and 2 GPa will not be attempted at 3 GPa. Instead, only the general trend of the liquid path will be given. Despite these uncertainties, it is expected that only the details of the fractional crystallization path would be changed by additional data, not the general trend.

Liquid V, in equilibrium with forsterite, diopside, enstatite, spinel, and garnet, is the liquid on the solidus of model lherzolite at the transition between spinel lherzolite and garnet lherzolite (Fig. 2). It is an invariant point in pressure-temperature space and lies very close to and probably slightly to the silica-poor side of the aluminous pyroxene thermal divide, $MgSiO_3$-$CaSiO_3$-Al_2O_2 (MILHOLLAND and PRESNALL, 1998). This explains why six univariant lines meet at V rather than four (Fig. 6), as is the case for the other points that are isobarically invariant.

As discussed by MILHOLLAND and PRESNALL (1998), the liquid path from V initially extends along the spinel-diopside surface toward the vicinity of W (Figs. 6, 7), but existing data are inadequate to determine whether the path curves back into the V–W univariant line or intersects W–O. In the latter case, the path could miss W entirely and move toward X along some path other than W–X. In general, however, the liquid path must extend along or near the left and top sides of the garnet-diopside surface defined by V–W–X–L–M. Garnet and clinopyroxene are major phases crystallizing along at least part of this path in addition to spinel, sapphirine, corundum, kyanite, and quartz. After arriving at M, the liquid path moves toward N and out of the tetrahedron. However, the position of N is poorly known and it may lie outside the FADS tetrahedron. Therefore, the liquid path beyond M is uncertain and M is the most fractionated liquid that can be deduced from this phase diagram.

Effect of Pressure on Cumulate Assemblages and Residual Liquid Compositions

At 1 atm, familiar mineral assemblages are crystallized. Initial forsterite crystallization is followed successively by forsterite + anorthite, forsterite + anorthite + diopside, diopside + enstatite + anorthite, and finally diopside + enstatite + anorthite + quartz (Fig. 8). At 2 GPa, three new phases, spinel, sapphirine, and garnet appear in the middle stages of

crystallization. Note in particular the segment from A to Y (Figs. 4, 8) along which garnet and diopside crystallize in approximately equal proportions. This shows that eclogites can form as cumulate assemblages at pressures as low as 2 GPa from moderately evolved magmas of intermediate SiO_2 content. Also note that sapphirine crystallizes along the R–A segment at 2 GPa. This indicates that sapphirine plays a role in the fractional crystallization of basaltic magmas at intermediate pressures, an issue that has been extensively discussed elsewhere (LIU and PRESNALL, 1990, in press). At 3 GPa, garnet and diopside are dominant minerals that crystallize throughout most or all of the fractionation path. Minor minerals that also crystallize are spinel, sapphirine, corundum, and kyanite. Broadly, the crystallizing assemblages are eclogitic, but a thorough understanding of the phase relations at this pressure requires more detailed data.

Despite strong differences in the phase relations at different pressures, it can be seen (Fig. 8) that the fractionation trends at all pressures show enrichment in SiO_2, depletion in MgO, and relatively little change in CaO. However, several notable differences occur. The maximum amount of SiO_2 enrichment decreases sharply from 1 atm to 2 GPa. The seemingly small change in maximum SiO_2 enrichment at higher pressures from 2 to 3 GPa may not be real because point M (Figs. 6, 7, 8) appears not to be the final residual liquid at 3 GPa. Although strong depletion of residual liquids in MgO occurs at all pressures, increasing pressure accentuates this decrease. At 1 atm, CaO is initially enriched because diopside does not crystallize. Then when diopside appears at h (Fig. 8), CaO decreases during the last half of the crystallization path. At 2 GPa, diopside begins to crystallize early, which prevents early enrichment of CaO. Alumina, which is strongly controlled by anorthite, shows a slight decrease in residual liquids at 1 atm but high pressures cause this trend to be reversed and the amount of Al_2O_3 increase is greatest at the highest pressure. At 1 atm, Al_2O_3 is initially enriched while forsterite is the only crystallizing phase from V to g (Fig. 8). Then crystallization of anorthite for the remainder of the liquid path causes a continuous decrease in Al_2O_3. At 2 GPa, anorthite appears late at point Y, which allows Al_2O_3 to increase during the early and middle stages of crystallization. After the appearance of anorthite, Al_2O_3 and CaO both decrease.

As discussed by LIU and PRESNALL (in press), the trend of SiO_2 enrichment at 2 GPa (Fig. 8) is at odds with the arguments of O'HARA and MERCY (1963), GREEN and RINGWOOD (1964, 1967), and O'HARA (1965) that increased crystallization of enstatite with increasing pressure results in the production of alkalic magmas by fractional crystallization of tholeiitic magmas. This difference occurs because crystallization of spinel (Fig. 8), which is important in producing the SiO_2 enrichment trend in the FADS tetrahedron at 2 GPa, was not considered in the earlier discussions. As liquid paths in the CMAS system cannot be considered completely definitive for complex natural magma compositions, resolution of this issue must await further data.

MID-OCEAN RIDGE BASALTS

Figure 9 shows a very dense and elongated array of mid-ocean ridge basalt glass (MORB) compositions (MELSON, 1992). A variety of chemical, mineralogical, and experimental evidence indicates that the pronounced trend toward the quartz apex is due to fractional crystallization of olivine, clinopyroxene, and plagioclase to produce residual liquids enriched in normative quartz (CLAGUE and BUNCH, 1976; BRYAN and MOORE, 1977, WALKER *et al.*, 1979; PRESNALL and HOOVER, 1987; O'DONNELL and PRESNALL, 1980, ELTHON and SCARFE, 1984; PRESNALL and HOOVER, 1984, 1987; TORMEY *et al.*, 1987). Using an older compilation by MELSON (1977), MCKENZIE and O'NIONS (1998, p. 147) asserted that the elongation is due entirely to small differences in Na_2O and is unrelated to fractional crystallization, but this con-

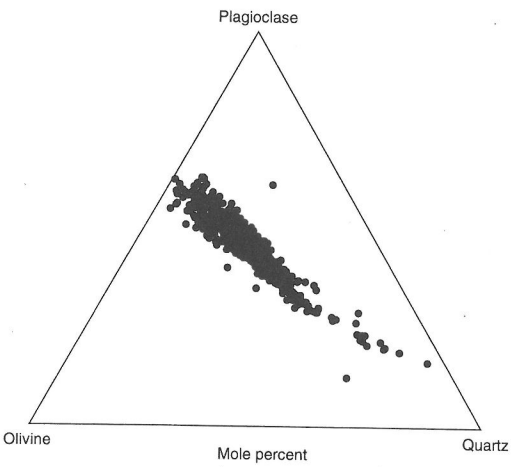

FIG. 9. Molecular CIPW normative plot of MORB glasses. Data are 1233 microprobe analyses of submarine samples with ages less than 1 my (MELSON, 1992), and include samples from the Pacific, Atlantic, and Indian Oceans. Ten omitted analyses from MELSON (1992) are nepheline normative. For all analyses, $Fe^{2+}/(Fe^{2+} + Fe^{3+})$ is normalized to 0.9. Olivine, $Mg_2SiO_4 + Fe_2SiO_4$; plagioclase, $CaAl_2Si_2O_8 + Na_2Al_2Si_6O_{16}$; quartz, SiO_2. Normative hypersthene in the CIPW norm is distributed between olivine and quartz.

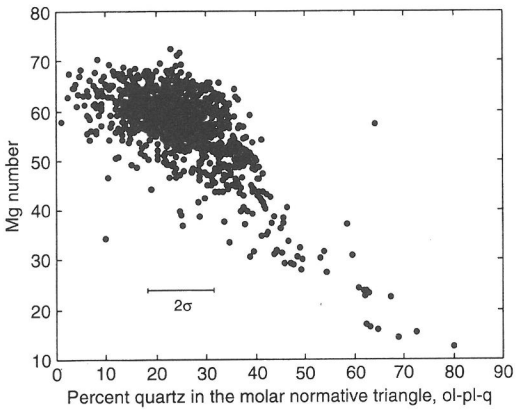

FIG. 10. Mg number, $Mg/(Mg + Fe^{2+})$, versus percent quartz, normalized to 100% olivine + plagioclase + quartz, in MORB glasses (MELSON, 1992). In calculating percent quartz, hypersthene is divided between olivine and quartz in the CIPW norm.

clusion was significantly preordained by their elimination of the most fractionated samples with MgO<4%. They used the normative triangle, olivine-diopside-quartz rather than olivine-plagioclase-quartz, but the disagreement applies equally to both diagrams.

PRESNALL and HOOVER (1984, 1987) showed, for a limited number of Atlantic MORBs, that the Mg number generally decreases as normative quartz, as represented in Fig. 9, increases. Figure 10 demonstrates that this correlation holds even more strongly for the much larger worldwide database of MORB analyses assembled by MELSON (1992). Thus, there can be no question that compositions along the trend change in a way that is consistent with fractional crystallization. Even if the more fractionated samples with MgO<4% were eliminated, as done by MCKENZIE and O'NIONS (1998), the left-hand portion of the trend in Fig. 10 at <50% normative quartz would remain.

During fractional crystallization, Na_2O increases in the residual liquid, but PRESNALL *et al.* (1979, p. 21) emphasized that addition of Na_2O to a composition plotted in Fig. 9 moves it away from the SiO_2 apex, opposite to the trend of fractional crystallization indicated by the decreasing Mg number and increasing SiO_2 content. Thus, the Na_2O problem of MCKENZIE and O'NIONS (1998) causes blurring of the fractionation trend in Figs. 9 and 10 but does not negate it.

In an experimental study of North Atlantic MORBs at 1 atm, GROVE and BRYAN (1983) found a crystallization sequence of olivine, then olivine + plagioclase, and finally olivine + plagioclase + augite. With the exception of spinel, which they found in some of their experiments, this is exactly the sequence of phases that crystallizes along the V–g–h–p path at 1 atm (Figs. 3, 8, 11). Furthermore, the 1 atm CMAS fractionation trend that includes points g–h–p–e (Fig. 11) lies precisely along the MORB trend. The close agreement of the experimental study of natural compositions by GROVE and BRYAN (1983) and the model system calculations shown here clearly establishes that the MORB array shown in Fig. 9 is dominantly caused by fractional crystallization at very low pressures.

As shown in Figs 12 and 13, liquid paths at higher pressures cut across the MORB array, which argues against a *dominant* role for fractional crystallization at higher pressures. However, note that the middle part of the liquid path at 2 GPa from R to Y (Fig. 12) cuts across the MORB array at a small angle. Thus, crystallization at higher pressures cannot be completely ignored. With this in mind, it is interesting

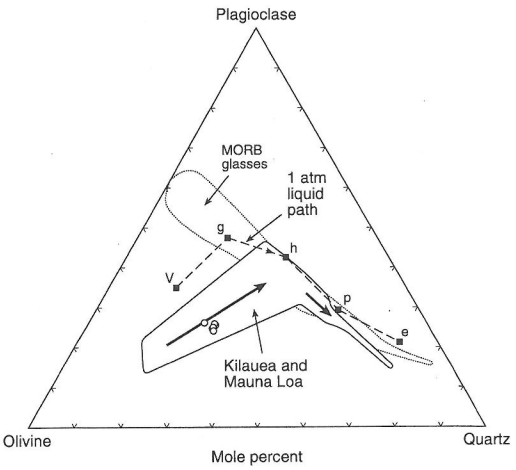

FIG. 11. Molecular CIPW normative plot projected from diopside, $CaMgSi_2O_6$. Labeled points on the liquid paths for fractional crystallization at 1 atm. are the same as in Figs. 3 and 8. The Kilauea and Mauna Loa, Hawaii, field shows the approximate boundary for high quality wet chemical analyses of 282 whole rock and 7 glass samples performed at the U. S. Geological Survey rock analysis laboratory in Denver (MACDONALD, 1955a, 1955b; MACDONALD and EATON, 1955; MUIR and TILLEY, 1957; MURATA and RICHTER, 1961, 1966; RICHTER *et al.*, 1964; MOORE and AULT, 1965; MOORE, 1965, 1966; PECK *et al.*, 1966; MOORE and EVANS, 1967; FISKE and KOYANAGI, 1968; WRIGHT *et al.*, 1968; KINOSHITA *et al.*, 1969; MOORE and KOYANAGI, 1969; WRIGHT, 1971; WRIGHT and FISKE, 1971) plus 60 microprobe analyses of Kilauea glasses from CLAGUE *et al.* (1995). Six of the most magnesian glass compositions from CLAGUE *et al.* (1995) are shown as open circles. Heavy arrows in the Hawaii field indicate directions of fractional crystallization. The MORB glass field is from Fig. 9 and omits 5 outliers.

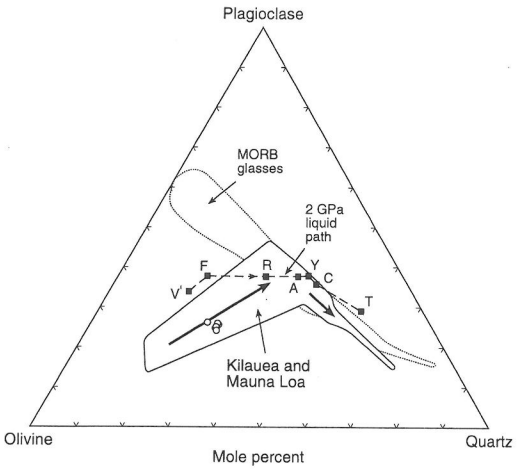

FIG. 12. Same as Fig. 11 but showing the liquid path for fractional crystallization at 2 GPa. Labeled points are the same as in Figs. 4, 5, and 8.

that the width of the MORB array increases with decreasing normative quartz. This increase may be caused by crystallization of less fractionated magmas at an angle to the main array at greater than oceanic crustal pressures. This possibility was also suggested on the basis of least squares mixing calculations involving high-pressure crystallization of clinopyroxene (O'DONNELL and PRESNALL, 1980).

HAWAIIAN THOLEIITES

In contrast to MORBs, tholeiitic basalts from Kilauea and Mauna Loa volcanoes in Hawaii show a strong initial fractionation trend controlled by crystallization only of olivine followed by late crystallization of olivine, clinopyroxene, plagioclase, orthopyroxene, and pigeonite (Fig. 11). The broad band of olivine-controlled compositions for Mauna Loa and Kilauea is actually composed of two overlapping trends, with the Mauna Loa trend being slightly richer in normative quartz than that for Kilauea. Also, for Kilauea, the overall trend, when broken into time segments, is itself composed of three trends that radiate out from the olivine apex along tightly controlled olivine control lines (WRIGHT, 1971). Glass analyses from Mauna Loa and Kilauea duplicate the Hawaiian array in Fig. 11 except for the most magnesian portion of the olivine-controlled trend. The open circles are the most magnesian glasses that have been reported in Hawaii (CLAGUE *et al.*, 1995), and they lie well outside the field of MORB glasses. Thus, the difference between the MORB and Hawaiian trends is not caused by the dominance of whole rock compositions in the latter.

Whole rock compositions in the olivine-controlled portion of the Hawaiian trend are influenced strongly by abundant olivine phenocrysts, and there has been much debate about the amount of olivine that may have once been part of the parental melt (*e.g.*, WILKINSON and HENSEL, 1988; GARCIA *et al.*, 1995). Estimates for the amount of MgO in parental magmas have ranged widely from 25% (WRIGHT, 1984) to 8% (MAALØE, 1979); but glass analyses from Kilauea with 15% MgO (CLAGUE *et al.*, 1991, 1995) demonstrate that parental picritic magmas at least this magnesian must exist. The fact that the olivine controlled portion of the Hawaiian trend (Fig. 11) is displaced from the olivine-controlled portion (V–g) of the CMAS trend is of no significance except to indicate that the CMAS trend assumes a starting composition displaced slightly from the parental magmas that produced the Hawaiian trend. A starting composition could have been chosen that would follow precisely along the Hawaiian trend.

The olivine-controlled portion of the Hawaiian trend could form in two ways. On the assumption that the parental magmas are picritic, olivine control could be maintained by polybaric crystallization of olivine during ascent from the source region. It would be necessary only that the rate of ascent be sufficiently rapid to keep the crystallizing magma composition within the expanding olivine primary phase volume. Alternatively, the magma could rise rapidly with little or no crystallization during ascent and the bulk of the olivine controlled trend would be produced by olivine crystallization at very low pressures.

The more fractionated portion of the Hawaiian trend is essentially identical to the more fractionated

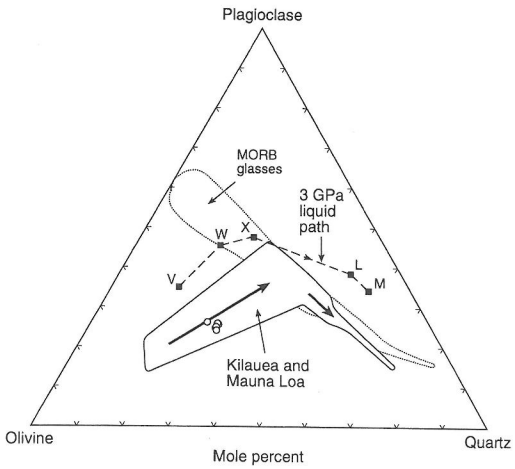

FIG. 13. Same as Fig. 11 but showing the liquid path for fractional crystallization at 3 GPa. Labeled points are the same as in Figs. 6, 7, and 8.

part of the MORB trend and to the 1 atm CMAS trend from h to e (Fig. 11). This strongly supports the conventional view that basalts in Hawaii as well as at spreading ridges are extensively fractionated at shallow depths. The strong difference between MORBs and Hawaiian tholeiites in the early stages of fractionation indicates a significant difference between the two starting compositions. If it is assumed that both parental magma types are generated from a lherzolitic mantle source, the simplest way to produce different parental compositions is to generate them from strongly different pressure regimes in which the phase relations differ. However, this very interesting subject is beyond the scope of the present discussion of fractional crystallization processes.

HIGH Al_2O_3 BASALTS AND ANDESITES

As described above for Hawaii and mid-ocean ridges, lavas of different compositions erupted at the Earth's surface can frequently be related by low-pressure fractionation processes. However, if high pressure fractionation gives liquid paths that have broad similarities to low pressure liquid paths, as Fig. 8 shows to be the case, then these high pressure processes may be masked, particularly if the crystals formed at high pressures subsequently dissolve or are separated from the residual liquids as they rise to the Earth's surface. In many cases, the only remaining evidence would be minor differences in lava compositions. It is just this kind of subtle evidence that has driven much of the discussion about island arc lavas. High alumina basalts and andesites from island arcs are generally higher in Al_2O_3 and lower in MgO than fractionated Hawaiian basalts that have reached saturation with olivine, clinopyroxene, and plagioclase; and SISSON and GROVE (1993a, 1993b) have shown experimentally that the compositions of these island arc lavas are consistent with fractionation under hydrous conditions that include crystallization of amphibole at pressures of roughly 0.2 GPa (see also an earlier review by CAWTHORN and O'HARA, 1976). However, DRAPER and JOHNSON (1992) have argued that high-alumina basalts can also be produced by high pressure (<1.5 GPa) fractional crystallization under anhydrous conditions. The data given here show that residual liquids high in Al_2O_3 and low in MgO can be produced over a wide pressure range under anhydrous conditions. Thus, although subduction zone magmas are commonly or universally hydrous and amphibole is a frequent crystallization product, high pressure appears to be a more important factor in producing the observed high Al_2O_3 and low MgO characteristics of these magmas by fractional crystallization.

Acknowledgments—It is a great pleasure to be able to contribute to this volume in tribute to the remarkable career of Joe Boyd. Manuscript preparation was supported by National Science Foundation grant EAR-9725900 and Texas Advanced Research Program grant 009741-046. I thank Leslie Yale for her assistance in preparing the plots of MORB glasses, John Dalton and Dave Draper for very useful comments on a preliminary version of the manuscript, and Michael Walter and Jürgen Konzett for their constructive editorial reviews. Department of Geosciences, University of Texas at Dallas contribution no. 893.

REFERENCES

ANDERSEN O. (1915) The system anorthite-forsterite-silica. *Am. J. Sci.* **39,** 407–454.

BOWEN N. L. (1914) The ternary system diopside-forsterite-silica. *Am. J. Sci.* **38,** 207–264.

BRYAN W. B. and MOORE J. G. (1977) Compositional variations of young basalts in the Mid-Atlantic Ridge rift valley near lat. 36°49'N. *Geol. Soc. Am. Bull.* **88,** 556–570.

CAWTHORN R. G. and O'HARA M. J. (1976) Amphibole fractionation in calc-alkaline magma genesis. *Am. J. Sci.* **276,** 309–329.

CLAGUE D. A., WEBER W., and DIXON J. E. (1991) Picritic glasses from Hawaii. *Nature* **353,** 553–556.

CLAGUE D. A. and BUNCH T. E. (1976) Formation of ferrobasalt at east Pacific mid-ocean spreading centers. *J. Geophys. Res.* **81,** 4247–4256.

CLAGUE D. A., MOORE J. G., DIXON J. E., and FRIESEN W. B. (1995) Petrology of submarine lavas from Kilauea's Puna Ridge, Hawaii. *J. Petrol.* **36,** 299–349.

CLARK S. P. JR., SCHAIRER J. F., and DE NEUFVILLE J. (1962) Phase relations in the system $CaMgSi_2O_6$-$CaAl_2SiO_6$-SiO_2 at low and high pressure. *Carnegie Inst. Washington Year Book* **61,** 59–68.

DAVIS B. T. C. and SCHAIRER J. F. (1965) Melting relations in the join diopside-forsterite-pyrope at 40 kilobars and at one atmosphere. *Carnegie Inst. Washington Year Book* **64,** 123–126.

DRAPER D. S. and JOHNSON A. D. (1992) Anhydrous PT phase relations of an Aleutian high-MgO basalt: an investigation of the role of olivine-liquid reaction in the generation of arc high-alumina basalts. *Contrib. Mineral. Petrol.* **112,** 501–519.

ELTHON D. and SCARFE C. M. (1984) High-pressure phase equilibria of a high-magnesia basalt and the genesis of primary oceanic basalts. *Am. Mineral.* **69,** 1–15.

FISKE R. W. and KOYANAGI R. Y. (1968) The December 1965 eruption of Kilauea volcano, Hawaii. *U. S. Geol. Survey Prof. Paper* **607,** 21 pp.

GARCIA M. O., HULSEBOSCH T. P., and RHODES J. M. (1995) Olivine-rich submarine basalts from the Southwest Rift Zone of Mauna Loa volcano: Implications for magmatic processes and geochemical evolution. In *Mauna Loa Revealed* (eds. J. M. RHODES and J. P. LOCKWOOD), pp. 219–239, Geophys. Mon. **92,** Am. Geophys. Union, Washington, DC.

GASPARIK T. (1984) Two-pyroxene thermobarometry with new experimental data in the system CaO-MgO-Al_2O_3-SiO_2. *Contrib. Mineral. Petrol.* **87,** 87–97.

GREEN D. H. and RINGWOOD A. E. (1964) Fractionation of basalt magmas at high pressures. *Nature* **210,** 1276–1279.

GREEN D. H. and RINGWOOD A. E. (1967) The genesis of basaltic magmas. *Contrib. Mineral. Petrol.* **15,** 103–190.

GROVE T. L. and BRYAN W. B. (1983) Fractionation of pyroxene-phyric MORB at low pressure: An experimental study. *Contrib. Mineral. Petrol.* **84,** 293–309.

GUDFINNSSON G. H. and PRESNALL D. C. (1996) Melting relations of model lherzolite in the system CaO-MgO-Al_2O_3-SiO_2 at 2.5–3.4 GPa and the generation of komatiites. *J. Geophys. Res.* **101,** 27,701–27.709.

HERZBERG C. T. (1972) Stability fields of plagioclase- and spinel-lherzolite, in *Progress in Experimental Petrology* (eds. C. M. B. HENDERSON and D. L. HAMILTON), pp. 145–148, Natural Environment Research Council, Pub. Ser. D, No. 2.

HERZBERG C. T. (1992) Depth and degree of melting of komatiite. *J. Geophys. Res.* **97,** 4521–4540.

HERZBERG C. and O'HARA M. J. (1998) Phase equilibrium constraints on the origin of basalts, picrites, and komatiites. *Earth Sci. Rev.* **44,** 39–79.

HERZBERG C. and ZHANG J. (1997) Melting experiments on komatiite analog compositions at 5 GPa. *Am. Mineral.* **82,** 354–367.

HYTÖNEN K. and SCHAIRER J. F. (1961) The plane enstatite-anorthite-diopside. *Carnegie Inst. Washington Year Book* **59,** 71–72.

KINOSHITA W. T., KOYANAGI R. Y., WRIGHT T. L., and FISKE R. S. (1969) Kilauea volcano: The 1967–68 summit eruption. *Science* **166,** 459–468.

KORZHINSKII D. S. (1959) *Physicochemical Basis of the Analysis of the Paragenesis of Minerals.* Consultants Bureau, Inc., New York.

KUSHIRO I. (1968) Compositions of magmas formed by partial zone melting of the Earth's upper mantle. *J. Geophys. Res.* **73,** 619–634.

KUSHIRO I. (1969) The system forsterite-diopside-silica with and without water at high pressures. *Am. J. Sci.* **267A,** 269–294.

KUSHIRO I. (1972) Determination of liquidus relations on synthetic silicate systems with electron probe analysis: The system forsterite-diopside-silica at 1 atmosphere. *Am. Mineral.* **57,** 1260–1271.

KUSHIRO I. (1975) On the nature of silicate melt and its significance in magma genesis: Regularities in the shift of the liquidus boundaries involving olivine, pyroxene, and silica minerals. *Am. J. Sci.* **275,** 411–431.

KUSHIRO I. (1979) Fractional crystallization of basaltic magma. In *The Evolution of the Igneous Rocks: Fiftieth Anniversary Perspectives.* (ed. H. S. YODER, Jr.), pp. 171–203, Princeton Univ. Press.

KUSHIRO I. and SCHAIRER J. F. (1963) New data on the system diopside-forsterite-silica. *Carnegie Inst. Washington Year Book* **62,** 95–103.

LIBOUREL G., BOIVIN P., and BIGGAR G. M. (1989) The univariant curve liquid = forsterite + anorthite + diopside in the system CMAS at 1 bar: solid solutions and melt structure. *Contrib. Mineral. Petrol.* **102,** 406–421.

LIU T.-C. and PRESNALL D. C. (1990) Liquidus phase relationships on the join anorthite-forsterite-quartz at 20 kbar with applications to basalt petrogenesis and igneous sapphirine. *Contrib. Mineral. Petrol.* **104,** 735–742.

LIU T. C. and PRESNALL D. C. (in press) Liquidus phase relations in the system CaO-MgO-Al_2O_3-SiO_2 at 2.0 GPa: Applications to basalt fractionation, eclogites, and igneous sapphirine. *J. Petrol.*

LIU T.-C. and PRESNALL D. C. (1989) Diopside-tridymite liquidus boundary line in the system Mg_2SiO_4-$CaMgSi_2O_6$-SiO_2 at atmospheric pressure. *Am. Mineral.* **74,** 1032–1037.

LONGHI J. (1987) Liquidus equilibria and solid solution in the system $CaAl_2Si_2O_8$-Mg_2SiO_4-$CaSiO_3$-SiO_2 at low pressure. *Am. J. Sci.* **287,** 265–331.

LONGHI J. and HAYS J. F. (1979) Phase equilibria and solid solution along the join $CaAl_2Si_2O_8$-SiO_2. *Am. J. Sci.* **279,** 876–890.

MAALØE S. (1979) Compositional range of primary tholeiitic magmas evaluated from major element trends. *Lithos* **12,** 59–72.

MACDONALD G. A. (1955a) *Hawaiian Islands.* Part 3 of Catalog of the Active Volcanoes of the World, Int. Volcanological Assoc., Napoli, Italy.

MACDONALD G. A. (1955b) Hawaiian volcanoes during 1952. *U. S. Geol. Survey Bull.* **1021-B,** 15–108.

MACDONALD G. A. and EATON J. P. (1955) Hawaiian volcanoes during 1953, *U. S. Geol. Survey Bull.* **1021-D,** 127–166.

MCKENZIE D. and O'NIONS R. K. (1998) Melt production beneath oceanic islands. *Phys. Earth Planet. Int.* **107,** 143–182.

MELSON W. G., BYERLY G. R., NELEN J. A., O'HEARN T., WRIGHT T. L., and VALLIER T. (1977) A catalog of the major element chemistry of abyssal volcanic glasses. In *Mineral Sciences Investigations, 1974–1975.* (ed. B. MASON), pp. 31–60, Smithsonian Contrib. Earth Sci. **19.**

MELSON W. G. (1992) *VGGP Database of Basalt Glass Analyses.* Smithsonian Institution, Washington, D. C.

MILHOLLAND C. S. and PRESNALL D. C. (1998) Liquidus phase relations in the CaO-MgO-Al_2O_3-SiO_2 system at 3.0 GPa: the aluminous pyroxene thermal divide and high-pressure fractionation of picritic and komatiitic magmas. *J. Petrol.* **39,** 3–27.

MOORE J. G. (1965) Petrology of deep-sea basalt near Hawaii. *Am. J. Sci.* **263,** 40–52.

MOORE, J. G. (1966) Rate of palagonitization of submarine basalt adjacent to Hawaii. *U. S. Geol. Survey Prof. Paper* **550-D,** D163–D171.

MOORE J. G. and AULT W. U. (1965) Historic littoral cones in Hawaii. *Pacific Science* **19,** 3–11.

MOORE J. G. and EVANS B. W. (1967) The role of olivine in the crystallization of the prehistoric Makaopuhi tholeiitic lava lake, Hawaii. *Contrib. Mineral Petrol.* **15,** 202–223.

MOORE J. G. and KOYANAGI R. Y. (1969) The October 1963 eruption of Kilauea volcano, Hawaii. *U. S. Geol. Survey Prof. Paper* **614–C.**

MUAN A. and OSBORN E. F. (1956) Phase equilibria at liquidus temperatures in the system MgO-FeO-Fe_2O_3-SiO_2. *Am. Ceramic Soc. J.* **39,** 121–140.

MUIR I. D. and TILLEY C. E. (1957) The picrite-basalts of Kilauea, Pt. 1 of Contributions to the petrology of Hawaiian basalts. *Am. J. Sci.* **255,** 241–253.

MURATA K. J. and RICHTER D. H. (1966) Chemistry of the lavas of the 1959–60 eruption of Kilauea volcano, Hawaii. *U. S. Geol. Survey Prof. Paper* **537-A,** A1–A26.

MURATA K. J. and RICHTER D. H. (1961) Magmatic differentiation in the Uwekahuna laccolith, Kilauea caldera, Hawaii. *J. Petrol.* **2,** 424–437.

O'DONNELL T. H. and PRESNALL D. C. (1980) Chemical variations of the glass and mineral phases in basalts dredged from 25°–30° N along the Mid-Atlantic Ridge. *Am. J. Sci.* **280-A,** 845–868.

O'HARA M. J. (1968) The bearing of phase equilibria studies in synthetic and natural systems on the origin and evolution of basic and ultrabasic rocks. *Earth-Science Rev.* **4,** 69–133.

O'HARA M. J. (1965) Primary magmas and the origin of basalts. *Scott. J. Geol.* **1,** 19–39.

O'HARA M. J. and MERCY E. L. P. (1963) Petrology and

petrogenesis of some garnetiferous peridotites. *Trans. Roy. Soc. Edinburgh* **65,** 251–314.

O'Hara M. J. and Yoder H. S. Jr. (1967) Formation and fractionation of basic magmas at high pressures. *Scott. J. Geol.* **3,** 67–117.

O'Hara M. J. and Yoder H. S. Jr. (1963) Partial melting of the mantle. *Carnegie Inst. Washington Year Book* **62,** 66–71.

O'Hara M. J., Richardson S. W., and Wilson G. (1971) Garnet-peridotite stability and occurrence in crust and mantle. *Contrib. Mineral. Petrol.* **32,** 48–68.

Osborn E. F. (1959) Role of oxygen pressure in the crystallization and differentiation of basaltic magma. *Am. J. Sci.* **257,** 609–647.

Osborn E. F. and Tait D. B. (1952) The system diopside-forsterite-anorthite. *Am. J. Sci.* **Bowen Vol.,** 413–433.

Peck D. L., Wright T. L., and Moore J. G. (1966) Crystallization of tholeiitic basalt in Alae lava lake, Hawaii. *Bull. Volcanol.* **29,** 629–655.

Presnall D. C. (1966) The join forsterite-diopside-iron oxide and its bearing on the crystallization of basaltic and ultramafic magmas. *Am. J. Sci.* **264,** 753–809.

Presnall D. C. (1976) Alumina content of enstatite as a geobarometer for plagioclase and spinel lherzolites. *Am. Mineral.* **61,** 582–588.

Presnall D. C. (1986) An algebraic method for determining equilibrium crystallization and fusion paths in multicomponent systems. *Am. Mineral.* **71,** 1061–1070.

Presnall D. C. (1991) Algebraic methods for determining directions of decreasing temperature along isobaric liquidus univariant lines. *Canadian Mineral.* **29,** 687–692.

Presnall D. C. and Hoover J. D. (1987) High pressure phase equilibrium constraints on the origin of mid-ocean ridge basalts. In *Magmatic Processes: Physicochemical Principles.* (ed. B. O. Mysen), pp. 75–89, Geochemical Soc. Spec. Pub. **1.**

Presnall D. C. and Hoover J. D. (1984) Composition and depth of origin of primary mid-ocean ridge basalts. *Contrib. Mineral. Petrol.* **87,** 170–178.

Presnall D. C., Dixon J. R., O'Donnell T. H., and Dixon S. A. (1979) Generation of mid-ocean ridge tholeiites. *J. Petrol.* **20,** 3–35.

Presnall D. C., Dixon S. A., Dixon J. R., O'Donnell T. H., Brenner N. L., Schrock R. L., and Dycus D. W. (1978) Liquidus phase relations on the join diopside-forsterite-anorthite from 1 atm to 20 kbar: Their bearing on the generation and crystallization of basaltic magma. *Contrib. Mineral. Petrol.* **66,** 203–220.

Richter D. H., Ault W. U., Eaton J. P., and Moore J. G. (1964) The 1961 eruption of Kilauea volcano, Hawaii. *U. S. Geol. Survey Prof. Paper* **474-D,** 34 pp.

Roeder P. L. and Osborn E. F. (1966) Experimental data for the system MgO-FeO-Fe_2O_3-$CaAl_2Si_2O_8$-SiO_2 and their petrologic implications. *Am. J. Sci.* **264,** 428–480.

Schairer J. F. and Kushiro I. (1964) The join diopside-silica. *Carnegie Inst. Washington Year Book* **63,** 130–132.

Shi P. and Libourel G. (1991) The effects of FeO on the system CMAS at low pressure and implications for basalt crystallization processes. *Contrib. Mineral. Petrol.* **108,** 129–145.

Sisson T. W. and Grove T. L. (1993a) Experimental investigations of the role of H_2O in calc-alkaline differentiation and subduction zone magmatism. *Contrib. Mineral. Petrol.* **113,** 143–166.

Sisson T. W. and Grove T. L. (1993b) Temperatures and H_2O contents of low-MgO high-alumina basalts. *Contrib. Mineral. Petrol.* **113,** 167–184.

Tormey D. R., Grove T. L., and Bryan W. B. (1987) Experimental petrology of normal MORB near the Kane Fracture Zone: 22°–25° N, mid-Atlantic ridge. *Contrib. Mineral. Petrol.* **96,** 121–139.

Walker D, Shibata T., and DeLong S. E. (1979) Abyssal tholeiites from the Oceanographer Fracture Zone II. Phase equilibria and mixing. *Contrib. Mineral. Petrol.* **10,** 111–126.

Walter M. J. and Presnall D. C. (1994) Melting behavior of simplified lherzolite in the system CaO-MgO-Al_2O_3-SiO_2-Na_2O from 7 to 35 kbar. *J. Petrol.* **35,** 329–359.

Wilkinson J. F. G. and Hensel H. D. (1988) The petrology of some picrites from Mauna Loa and Kilauea volcanoes, Hawaii. *Contrib. Mineral Petrol.* **98,** 326–345.

Wright T. L. (1971) Chemistry of Kilauea and Mauna Loa lavas in space and time. *U. S. Geol. Survey Prof. Paper* **735,** 40 pp.

Wright T. L. (1984) Origin of Hawaiian tholeiite: A metasomatic model. *J. Geophys. Res.* **89,** 3233–3252.

Wright T. L. and Fiske R. S. (1971) Origin of differentiated and hybrid lavas of Kilauea volcano, Hawaii. *J. Petrol.* **12,** 1–65.

Wright T. L., Kinoshita W. T., and Peck D. L. (1968) March 1968 eruption of Kilauea volcano and the formation of Makaopuhi lava lake. *J. Geophys. Res.* **73,** 3181–3205.

Yoder H. S. Jr. (1976) *Generation of Basaltic Magma.* Natl. Acad. Sci., Washington, D. C., 265 pp.

Yoder H. S. Jr. and Tilley C. E. (1962) Origin of basalt magmas: an experimental study of natural and synthetic rock systems. *J. Petrol.* **3,** 342–532.